Archives available at journals.mriindia.com

International Journal of Advanced Electrical and Electronics Engineering

ISSN: 2278-8948
Volume 14 Issue 02, 2025

Design and Analysis of an AI enabled Zero Voltage Switching Boost Converter for Standalone Photovoltaic Systems

[1]Werulkar A. S., [2]Kulkarni P.S.
[1]*Professor, Department of Electronics and Tel. Engineering*
St. Vincent Pallotti College of Engineering and Technology Nagpur, India
[2]*Professor, Department of Electrical Engineering,*
Visveswaraya National Institute of Technology,Nagpur, India
[1]*https://orcid.org/0009-0006-6774-4823,* [2]*pskulkarni@eee.vnit.ac.in*

Peer Review Information

Submission: 05 Nov 2025

Revision: 25 Nov 2025

Acceptance: 17 Dec 2025

Keywords

Solar PV System, Artificial Intelligence, Soft Switching, ZVS Boost Converter, Adaptive Control, Power Electronics, Multisim Simulation.

Abstract

In photovoltaic systems, the reliability of power conversion depends greatly on intelligent control of converter operation. This paper presents an AI-assisted Zero Voltage Switching (ZVS) step up or boost converter with an auxiliary resonant circuit designed for photovoltaic systems. Artificial Intelligence algorithms integrated with the ATMEGA32 microcontroller enable adaptive switching, predictive control, and dynamic optimization of converter parameters under varying solar and load conditions. This intelligent approach minimizes switching losses, improves transient response, and enhances overall system efficiency. Simulation and validation using Multisim 10 demonstrate superior performance and adaptability compared to conventional converters.

1. Introduction

Solar photovoltaic (PV) systems require efficient DC–DC power converters for maximum utilization of solar energy and effective charge control of storage batteries. Conventional boost converters, though widely used, face efficiency limitations due to high switching losses and high current stress on semiconductor switches.

To overcome these challenges, various methods such as zero voltage switching(ZVS) and zero current switching (ZCS) have been explored. Soft-switching converters reduce switching losses, electromagnetic interference (EMI), and increase overall power conversion efficiency. This research mainly focuses on the design and implementation of a ZVS boost converter topology controlled through an ATMEGA32 microcontroller, specifically aimed at standalone photovoltaic systems.

2. Literature Review

In various research studies, numerous scholars have suggested cost-effective and highly efficient designs for DC-DC Buck and Boost converters. The underlying power circuit typically includes a high step-up converter combined with a PWM inverter. This configuration enhances overall efficiency by enabling parallel operation of low-voltage photovoltaic (PV) modules, thus simplifying the PWM inverter's control mechanism [1]. A microcontroller-based optimal battery charging system has been developed with the aim of improving both battery lifespan and overall system efficiency [2]. To achieve maximum power extraction from PV modules, an intelligent microcontroller- controlled DC-DC converter has been implemented for Maximum Power Point (MPP) tracking. Additionally, a low-cost, battery-buffered PV power conditioning unit has been introduced,

prompting users to optimize configuration settings for enhanced energy generation. The charge controller employs a dynamic DC/DC converter topology regulated by a microcontroller to meet low-cost design requirements [3]. For rechargeable battery charging, a Zero Current Switching (ZCS) buck converter configuration is utilized. By incorporating an auxiliary switch in series with a resonant capacitor, the proposed ZCS buck DC-DC battery charger achieves substantial reduction in switching losses across active power components. This topology offers advantages such as simple structure, affordability, ease of control, and high efficiency [4]. Similarly, a Zero Voltage Switching (ZVS) resonant buck converter-based charger has been proposed to achieve low switching losses, high power density, and minimal electromagnetic interference [5]. Microcontroller-assisted resistive control for battery charging is discussed in [6], while [7] describes microprocessor-driven optimal battery chargers. The development of solar-powered battery chargers for NiMH batteries is detailed in [8], and [9] presents the design and implementation of a microprocessor-based battery charger integrated with a state-of-charge estimator. Energy performance analysis for a solar home lighting system using a microcontroller-based charge controller is provided in [10]. A detailed case study of a residential PV setup is investigated in [11], and [12] explores the design and functioning of microcontroller-based solar charge controllers.

In photovoltaic systems, the microcontroller-driven charge controller constitutes a vital subsystem. It leverages high- efficiency power conversion principles to minimize energy dissipation. Soft-switching DC-DC converters are crucial in determining the overall efficiency of PV systems since they effectively lower switching losses. Several converter

configurations—such as ZCS buck, ZVS boost, ZVS dual boost, and ZVS buck-boost—have been simulated, producing waveforms that satisfy soft-switching conditions. Furthermore, the ZVS boost converter has been evaluated for Maximum Power Point Tracking (MPPT) using the Perturb and Observe (P&O) technique. As Multisim software lacks MPPT simulation capabilities, Matlab has been employed for simulation and performance analysis.

I. ANALYSIS OF ZVS BOOST CONVERTER FOR SHLS

The proposed ZVS boost converter employs:

Main Switch (S1): IRF250 MOSFET.

Auxiliary Switch (S2): IRF250 MOSFET.

Resonant Components: Resonant inductor (Lr) and capacitor (Cr).

Controller: ATMEGA32 microcontroller to give necessary switching pulses.

Fig.1 shows schematic diagram of soft switching boost converter.

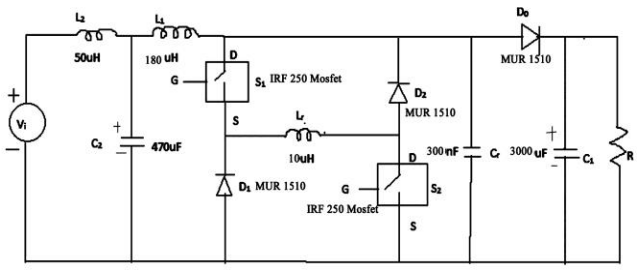

Fig.1: Circuit diagram of soft switching boost c onverter

Operating Principle:

The auxiliary resonant network enables zero-current switching (ZCS) during the switch-on period and zero-voltage switching (ZVS) during switch-off. The converter functions through six distinct operating modes that alternate between inductor energy storage, resonant transitions, and energy delivery to the load. Theoretical waveform analysis confirms minimized switching stresses and enhanced overall efficiency.

To enhance the energy conversion efficiency in photovoltaic (PV) systems, a soft-switching boost converter has been implemented. This topology incorporates a primary switching device supported by a simple auxiliary resonant circuit consisting of an auxiliary switch, diode, resonant inductor, and resonant capacitor. Traditional boost converters typically suffer from reduced efficiency due to hard-switching losses that occur during the transition of switches between on and off states. In the proposed configuration, all switches achieve zero-current switching at turn-on through the resonant inductor and zero-voltage switching at turn-off via the resonant capacitor. This soft-switching behavior significantly reduces switching losses, as well as voltage and current stresses on the active components. Figure 1 presents the schematic of the soft-switching DC-DC boost converter used for the Solar Home Lighting System (SHLS). In this circuit, switches S1 and S2 are IRF250 MOSFETs, C1 and C2 are electrolytic capacitors, and Cr represents an AC resonant capacitor.

The control of the proposed converter is achieved through an ATMEGA32 microcontroller. Functionally, the ATMEGA16 and ATMEGA32 microcontrollers are nearly identical, with the main difference lying in their internal memory capacities—the ATMEGA16 provides 1120 bytes of data memory, while the ATMEGA32 offers 2144 bytes. The auxiliary resonant circuit comprises an auxiliary switch (S2), resonant capacitor (Cr), resonant inductor (Lr), and two diodes (D1 and D2). The converter operates in six distinct intervals. For analytical simplicity, the following assumptions are made:

1. All semiconductor switches and passive components are considered ideal.
2. The parasitic effects of all components are neglected.
3. The solar panel supplies an input voltage (Vs) in the range of 15 to 17.5 V under load.
4. The converter operates in continuous conduction mode (CCM) throughout all intervals.

Figure 2 illustrates the theoretical waveforms of the boost converter during its various operating stages.

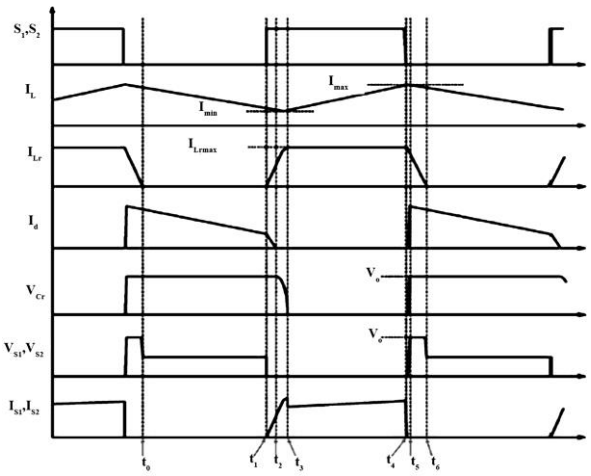

Fig.2:Theoretical waveforms

Assumptions:

All devices are ideal.

Input voltage: 15–17.5 V from PV module.

Continuous conduction mode operation.

3.1 Interval 1 (t0 ≤ t < t1)

- In this operating mode, both switches S1 and S2 remain in the OFF state. No current passes through either switch, and the energy stored in the main inductor is delivered to the load. The corresponding

operating modes are illustrated in Fig. 3. During this period, the current in the main inductor decreases linearly, while no current flows through the resonant inductor. Eventually, the resonant capacitor becomes charged to the level of the output voltage.

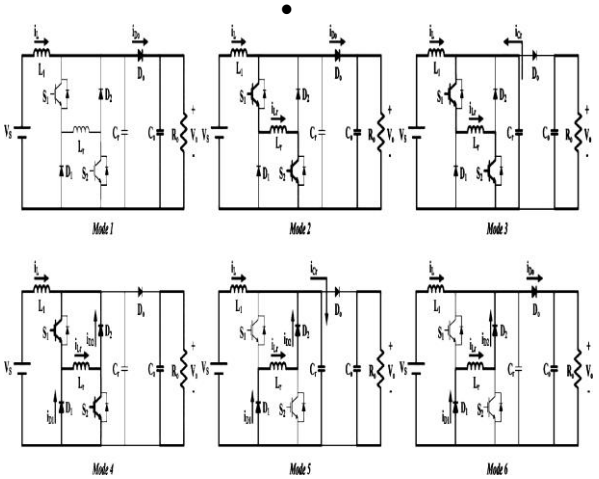

Fig. 3 Operational modes of the soft-switching boost converter for the PV generation system.

After turning on the two switches, interval 1 is over. These conditions are described as follows:

$$V_L(t) = V_s - V_o \quad (4.11)$$

$$i_L(t) = i_L(t_o) - \frac{V_o - V_s}{L} t \quad (1)$$

$$\begin{aligned} i_{Do}(t) &= i_L(t) \\ i_{Lr}(t) &= 0 \\ v_{cr}(t) &= V_o \end{aligned} \quad (2)$$

3.2 Interval 2 (t1 ≤ t < t2)

When switches S1 and S2 are turned ON, current begins to flow through the resonant inductor. As the current through both switches is zero at the instant of turn-on, the circuit operates under a zero-current switching (ZCS) condition. This ZCS feature significantly reduces switching losses compared to conventional hard-switching converters. During this interval, the resonant current increases linearly while the load current gradually declines. At time t2t_2t2, the current in the main inductor becomes equal to that in the resonant inductor, resulting in zero current through the output diode. When the resonant capacitor voltage reaches the output voltage VoV_oVo, the output diode turns OFF, marking the end of interval 2.

$$\begin{aligned} &i_{Lr}(t_1) = 0, v_{Lr}(t) = Vo \\ &i_{Lr}(t) = \frac{V_o}{L_r}(t) \\ &i_L(t) = i_L(t_1) - \frac{V_o - V_s}{L}(t) \\ &i_L(t_2) = i_{Lr}(t_2) \\ &i_{Do}(t_2) = 0 \end{aligned} \quad (3)$$

3.3 Interval 3 (t2 ≤ t < t3)

The current which was flowing earlier to the load through output diode D_o *no* longer flows since t_2.After this resonant capacitor *Cr*, and the resonant inductor *Lr start* a resonance. The current flowing to the resonant inductor is addition of the main inductor current and the resonant capacitor current. The resonant current is expressed as

$$\begin{aligned} &i_L(t) = i_{\min} \\ &i_{Lr}(t) = i_{\min} + \frac{V_o}{Z_r}.\sin\omega_r \\ &v_{cr}(t) = V_o.\cos\omega_r t \\ &v_{cr}(t_2) = V_o, v_{cr}(t_3) = 0 \\ &\omega_r = \frac{1}{\sqrt{L_r.C_r}}, Z_r = \sqrt{\frac{L_r}{C_r}} \end{aligned} \quad (4.15)$$

This period is called as resonant period .During this period, the resonant capacitor C_r is discharged from V_o to zero. This is shown in (3).It also shows resonant frequency and impedance. When the voltage of the resonant capacitor becomes zero, the interval 3 is over

3.4 Interval 4 (t3 ≤ t < t4)

After completion of the resonant period in interval 3, the voltage of the resonant capacitor equals zero, and then interval 4 begins.

In this interval, the freewheeling diodes D1 and *D*2 are turned on, and the current of the resonant inductor reaches maximum. The resonant inductor current flow to the freewheeling diodes in the sequence S1−Lr−D2 and S2−Lr−D1 .This follows the freewheeling path.

$$\begin{aligned} &i_{Lr}(t) = i_L(t) + i_{D1}(t) + i_{D2}(t) \\ &i_{Lr}(t_3) = i_{Lr}(t_4) = i_{Lr\max} \\ &V_L(t) = V_s \\ &i_L(t) = i_{\min} + \frac{V_s}{L}. \end{aligned} \quad (4)$$

During this time, the main inductor voltage becomes equal to the input voltage. The current accumulating energy increases linearly

3.5 Interval 5 (t4 ≤ t < t5)

In **interval 5**, all switches are turned OFF under a **zero-voltage switching (ZVS)** condition facilitated by the resonant capacitor. During this phase, the initial values of the resonant inductor current and the resonant capacitor voltage are defined as expressed in equation (4). Once the switches are turned OFF, the resonant capacitor Cr begins charging up to the output voltage through the combined action of the two inductor currents. The output diode remains in the OFF state until the voltage across the resonant capacitor reaches Vo

$$\begin{aligned} & i_{Lr}(t_4) = i_{Lr\max} \\ & V_{cr}(t_4) = 0 \\ & i_L\ (t) = I_{\max} \\ & i_{Lr}(t) = I_{\max} - (I_{\max} + I_{Lr,\max}).\cos\omega_r t \\ & v_{Lr}(t) = Z_r.(I_{\max} + I_{Lr,\max}).\sin\omega_r t \\ & v_{cr}\ (t_5) = V_o \end{aligned} \quad (5)$$

3.6 Interval 6 (t5 ≤ t < t6)

Interval 6 starts when the voltage across the resonant capacitor becomes equal to the output voltage. After this point, the output diode Do turns ON under **zero-voltage switching (ZVS)** conditions. During this interval, both the main inductor current (I_L) and the resonant inductor current (I_{Lr}) conduct toward the load through the output diode Do, thereby completing the power transfer to the output.

$$\begin{aligned} & i_{Do}(t) = i_L(t) + i_{Lr}(t) \\ & i_{Lr}(t_5) = (I_{\max} + I_{Lr,\max}).\cos\omega_r(t_5 - t_4) - I_{\max} \\ & v_{Cr}(t) = V_o \end{aligned}$$

$$\begin{aligned} & i_L(t) = I_{\max} - \frac{V_o - V_s}{L_r}(t) \\ & i_{Lr}(\mathrm{t}) = i_{Lr}(t_6) - \frac{V_o}{L_r}(t) \\ & i_{Lr}(t_6) = 0 \end{aligned} \quad (7)$$

During this period, the currents through both inductors decrease linearly. Eventually, the energy stored in the resonant inductor is fully delivered to the load, marking the end of **interval 6**. The values of the resonant inductor (Lr) and resonant capacitor (Cr) are determined using the expressions given in equations (7) and (8).

$$L_r < \frac{(\frac{2}{\pi}D_{\min}.T.V_o - V_{FW}.D_{\max}.T)}{(\Delta i_L + \frac{2}{\pi}.I_{\min})} \quad (8)$$

$$C_r = \frac{0.04.D_{\min}^2.T^2}{\pi^2.L_r} + \frac{4.I_{\min}^2.L_r}{\pi^2.V_o^2} - \frac{0.8.I_{\min}.D_{\min}.T}{\pi^2.V_o} \quad (9)$$

Where, V_{FW}= freewheeling voltage drop, Δi_L = current ripple of main inductor, I_{min} = minimum current of main inductor, D_{min} = minimum duty cycle, D_{max} = maximum duty cycle, V_0 = output voltage.

The output of the DC-DC Boost converter is verified by connecting 10/20 W DC lamp load and different current and voltage waveforms are taken.

IV Simulation results

The DC-DC soft-switching converter was simulated using **Multisim 10** software, and the corresponding output waveforms were analyzed. The simulation schematic is illustrated in **Figure 4**. The soft-switching boost converter was modeled to obtain various waveform responses for parameters such as V_{DS1}_V_{DS2}, V_{Lr}_I_L, I_{Lr},I_D, I_{S1}, I_{S2}, V_{Cr}r, and the output boosted voltage V_O. **Figures 4 to 6** present the simulated waveforms of these parameters for the soft-switching DC-DC boost converter.

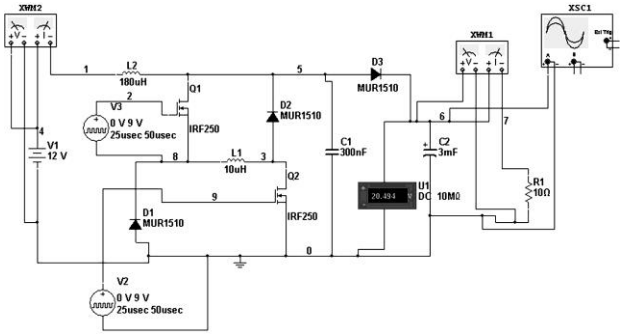

Fig. 4. Simulation diagram of ZVS boost converter using Multisim 10

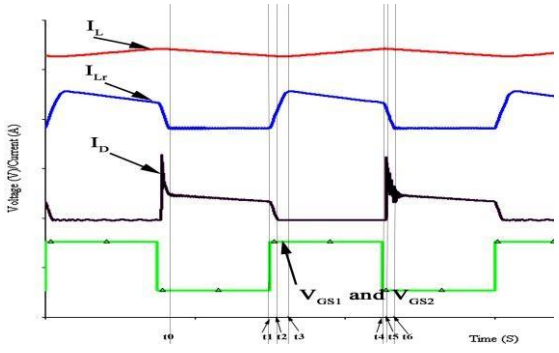

Fig.5. Waveform of main, resonant inductor current and output diode current

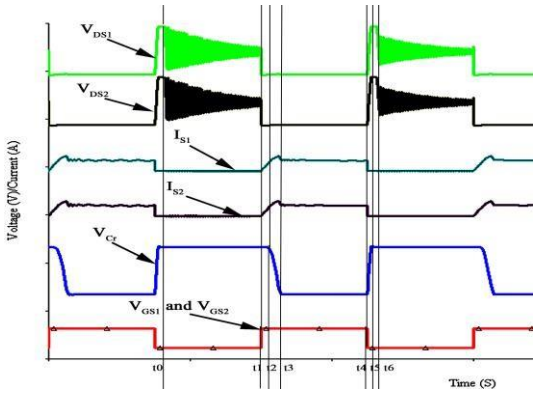

Fig. 6. Waveforms of voltages across switches (V_{DS1} and V_{DS2}), currents through switches S_1, S_2 (I_{S1} and I_{S2}) and voltage across resonant capacitor (V_{Cr})

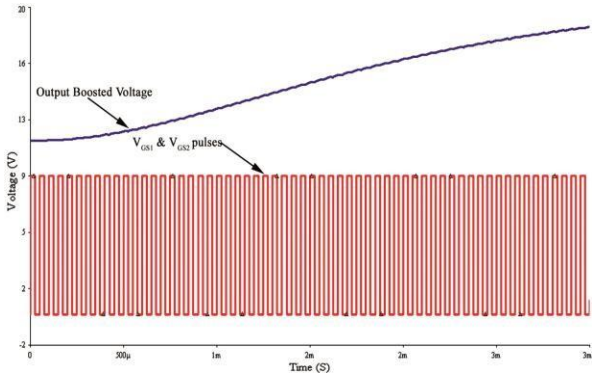

Fig. 7. Output boosted voltage as a function of switching pulses of switches

Fig.4 to 7 show various results of simulation for ZVS boost converter using multisim version 10 software

V. Results and Discussion

Simulation results show:

a) Reduced turn-on and turn-off losses due to ZVS conditions.

b) Lower current stress on MOSFETs.

c) Stable and efficient voltage boosting suitable for SHLS applications.

d) Microcontroller-based implementation provides adaptability for varying load and irradiance conditions.

VI. Conclusion

This paper presents the design and analysis of a ZVS boost converter for solar home lighting applications. The soft-switching approach significantly reduces switching losses, enhances efficiency, and prolongs the operational life of the converter. Future work includes hardware implementation and experimental validation of the proposed

Acknowledgment

The authors are thankful the authorities of Visveswaraya National Institute of Technology, Nagpur and St. Vincent Pallotti College of Engineering and Technology, Nagpur for carrying out research in the high efficiency soft switching power converter required for Solar PV system power conditioning units at the respective laboratories of power Electronics and Renewable Energy.

VI. Integration of AI in Proposed Converter

It is possible to integrate Artificial Intelligence (AI) into the proposed ZVS soft-switching boost converter for solar home lighting systems (SHLS). It can offer a transformative approach to achieve real-time optimization, adaptive topology.
control, and predictive performance enhancement of the system. In modern photovoltaic (PV)-based energy systems, there is a huge dynamics involved in solar irradiance, temperature, and load demand. This further introduce significant nonlinearities which a conventional rule-based or microcontroller-driven control algorithms can not handle efficiently. There are different AI-driven methodologies—such as machine learning (ML), fuzzy logic, and neural network-based predictive controllers. These can intelligently learn the system's behavior from data. In turn, they can continuously manage the converter's operating parameters to maintain optimal performance under varying environmental conditions. In other words, AI can enhance the converter's soft-switching operation by predicting the appropriate timing of Zero Voltage Switching (ZVS) transitions, thereby minimizing switching losses more effectively as compared to fixed-parameter control strategies. AI algorithms can be further implemented into the control loop of the ATMEGA32 microcontroller. This will enable adaptive pulse-width modulation (PWM) and real-time tracking of maximum power point (MPPT) with improved precision and reduced computational burden. This results in a converter which can operate efficiently also exhibits superior transient response and stability compared to traditional approaches.

Additionally, AI facilitates fault detection, diagnosis, and predictive maintenance within the converter circuit. By analyzing electrical parameters like current ripple, voltage waveforms, and temperature profiles, AI-based models can detect early signs of component degradation or abnormal operating conditions, allowing for proactive maintenance and increased system reliability. In the context of solar home lighting systems deployed in remote or rural areas, such predictive intelligence ensures uninterrupted operation, extended converter lifespan, and reduced maintenance costs. The use of AI-enabled data analytics also enables dynamic load forecasting and energy management, allowing the system to balance power conversion efficiency with lighting demand in a smart, self-regulating manner. Beyond hardware-level optimization, AI algorithms can analyze simulation and experimental data from Multisim 10 to fine- tune circuit

parameters, validate performance under different operating conditions, and recommend design improvements automatically through iterative learning. This integration of AI with simulation and experimental validation accelerates the design cycle and ensures that the converter achieves the best trade-off between efficiency, cost, and reliability.

The application of AI can not only enhances the technical performance of the ZVS boost converter but also align with global trends in intelligent renewable energy systems. It transforms the converter from a purely electronic device into a smart, adaptive energy interface capable of learning and self-optimization. Such a framework can be further extended to networked solar installations, where AI-enabled converters communicate and coordinate through IoT platforms for decentralized energy management. Therefore, embedding AI in the proposed ZVS soft-switching converter architecture ensures that the system is not only energy-efficient but also intelligent, resilient, and future-ready for next-generation solar home lighting applications.

References

[1] Hassan A.Khan n, SaadPervaiz "Technological review on solar PV in Pakistan: Scope, practices and recommendations for optimized system design" Renewable and Sustainable Energy Reviews 23, 2013,pp. 147–154

[2]H. Masheleni and X. F. Carelse, "Microcontroller-based charge controller for stand-alone photovoltaic systems" Solar Energy, Vol. 61, No. 4, 1997, pp. 225–230

[3] X. Long, R. Liao, J. Zhou "Low-cost charge collector of photovoltaic power conditioning system based dynamic DC/DC topology" IET Renew. Power Gener., Vol. 5, Iss. 2, 2011, pp. 167–174

[4]Y.C. Chuang Y.L. Ke "High efficiency battery charger with a buck zero-current-switching pulse-width-modulated converter", IET Power Electron., Vol. 1, No. 4, 2008, pp. 433–444

[5]Y. C. Chuang and Y. L. Ke, "High efficiency battery charger with a buck zero-current-switching pulse-width-modulated converter," *IET Power Electron.*, vol. 1, no. 4,
pp. 433–444, 2008.

[6] J. H. Lee, H. S. Bae, and B. H. Cho, "Resistive Control for a Photovoltaic Battery Charging System Using a Microcontroller" IEEE Transactions On Industrial Electronics, Vol. 55, No. 7, July 2008, pp. 2767-2775

[7] Mohamad A. S. Masoum, Seyed Mahdi Mousavi Badejani, and Ewald F. Fuchs, Fellow, IEEE "Microprocessor-Controlled New Class of Optimal Battery Chargers For Photovoltaic Applications", IEEE Transactions On Energy Conversion, Vol. 19, No. 3,
September 2004, pp.599-606

[8] Florent Boico, Brad Lehman, *a*nd Khalil Shujaee, "Solar Battery Chargers For Nimh Batteries", IEEE Transactions On Power Electronics, Vol. 22, No. 5, September 2007, pp.1600-1609

[9] Mohamad A. S. Masoum, Seyed Mahdi Mousavi Badejani, and Ewald F. Fuchs, Fellow, IEEE "Microprocessor-Controlled New Class of Optimal Battery Chargers For Photovoltaic Applications", IEEE Transactions On Energy Conversion, Vol. 19, No. 3, September 2004, pp.599-606

[10] Ashutosh S Werulkar, P. S. Kulkarni "Energy Analysis of Solar Home Lighting System with Microcontroller-based Charge Controller" Journal of Solar Energy Engineering, Transactions of ASME, August 2014, Vol. 136/031010-1 to 031010-9

[11] Ashutosh Sudhirrao Werulkar, Prakash S. Kulkarni "A Case Study of Residential Solar Photovoltaic System with Utility Backup in Nagpur, India" Renewable and Sustainable Energy Reviews, Elsevier Publications, 52 (2015) 1809–1822

[12] Vadla, A. K., "Microcontroller-Based Solar Charger," Electronics For You magazine, 2009.